# A SPH simulation of the sloshing phenomenon inside fuel tanks of the aircraft wings.

J. Calderon-Sanchez*, L.M. González
Universidad Politécnica de Madrid (UPM),
Madrid, Spain
* javier.calderon@upm.es,

S. Marrone, A. Colagrossi
CNR-INM, INstitute of Marine engineering,
Via di Vallerano 139, 00128 Rome, Italy

F. Gambioli
Airbus
Filton, England BS34 7PA, United Kingdom

***Abstract*—The wings of large civil passenger aircrafts, which are designed to withstand the loads occurring from atmospheric gusts and turbulence to landing impacts, still demand further research. This goal will be achieved through investigating the damping effect of sloshing on the dynamics of flexible wing-like structures carrying liquid via the development of experimental set-ups complemented by numerical models. The aim of this work is to analyze the effect of sloshing in reducing the design loads on aircraft structures using SPH as the main numerical tool. The first step of this research was performed inside the Airbus Protospace Lab in Filton (UK), where a scaled model of the problem was tested. The wing is represented by a cantilever with a liquid tank attached at its tip. The behaviour of the system once deformed and released and the accelerations at the free end of the beam were registered for different configurations.**

**In this work, a numerical model of a fully coupled fluid-structure interaction problem is developed. In order to understand and analyse the damping mechanisms, the structure is modelled through beam theory and solved by two different methods: a mass-spring-damper system and modal analysis. For the fluid, the $\delta$-LES-SPH model is used, which has been implemented for the boundary integrals methodology in order to simulate complex geometries.**

**A set of cases are simulated in order to reproduce trends noticed in the experiments, including different inner tank configurations, for the two beam models tested. SPH as numerical tool demonstrates that the presence of liquid in tanks attached to flexible structures introduces a damping effect.**

## I. Introduction

Challenges in aerospace industry, especially linked to the increase in passenger aircrafts size demands further research of associated systems that might influence craft behaviour when in operation. In particular, there is an interest in optimizing the wings of large civil passenger aircrafts , which are designed to withstand the loads occurring from atmospheric gusts and turbulence to landing impacts. This goal is aimed to be achieved through the investigation of the damping effect of sloshing on the dynamics of such wings in which the fuel is normally stored, through optimization of their inner configuration and analysis of liquid filling level.

A controlled sloshing has been proved to be effective in dampening movements in analogous structures, and examples can be found in civil engineering, through the design of Tuned Liquid Dampers (TLDs) that mitigate the motions in buildings when earthquakes occur [6, 19] , and in the naval industry, where anti-rolling tanks are widely used to minimize rolling motion of ships [17, 18].

These ideas have lately been considered within the aerospace industy for propellant rocket tanks, as it has been noted in [3] or in preliminary studies on sloshing on aircraft fuel tanks [12].

The present work aims to extend the knowledge on damping effects due to sloshing on aircraft wing tanks, by analysing the use of fuel slosh to reduce the design loads on aircraft structures. SPH will be used as the main numerical tool to reproduce sloshing. Previous analysis of this problem have been carried out in [4, 5], where a dynamical system consisting on an oscillating tank filled with fluid is studied. These works focus on understanding energy dissipation mechanisms, and a non-linear model for motion is used. Similarly, in this work the SPH tool will be complemented by a set of numerical models that reproduce wing motion, and are affected by the SPH computed sloshing loads. Results will be compared to experiments carried out inside the Airbus Protospace Lab in Filton (UK), where a simplified scaled model of the problem was tested. The simplified model arrangement can be seen in Figure 1. The test consists on the wing represented by a cantilever beam with a liquid tank attached at its tip. The beam is preloaded and released, and the accelerations at different points are recorded. Also the liquid motion is visually recorded at high speed rates in order to understand liquid slosh inside the tank. Different configurations were used, including different liquids, inner baffled configurations (both horizontally and vertically located) and filling levels are tested.

In this work, a numerical model of a fully coupled fluid-structure interaction problem is developed. In order to understand and analyse the damping mechanisms, the structure is modelled through the Euler-Bernouilli beam theory and solved by different means. Numerical methods such as finite

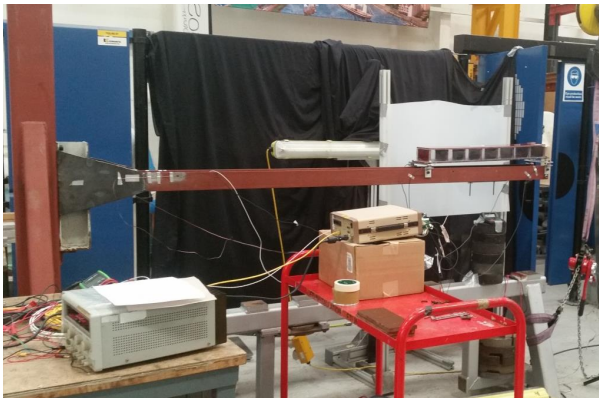

Fig. 1. Set-up of the experiments carried out at Airbus Protospace Lab in Filton (UK).

elements or SPH are avoided, and instead the beam is modelled by a simple mass-spring-damper system and by modal analysis [13]. For the fluid, the $\delta$-LES-SPH model is used [11, 14, 15], which has been implemented for the boundary integrals methodology developed in [7].

The paper is structured as follows: first, the $\delta$-LES-SPH model and the numerical models used for the beam are presented. The energy balance within the fluid and the beam is also presented in this Section. Second, both static and dynamic tests are performed with the different methods, and the results are compared with experiments. Similarities and differences found between both approaches, as well as the kindness of the numerical model when compared to the experiments are discussed. Finally, conclusions are drawn, and future work lines are established.

## II. Numerical model

### A. SPH model

The Navier-Stokes equations for a weakly-compressible and barotropic fluid can be written in Lagrangian form as:

$$\begin{cases} \dfrac{D\rho}{Dt} = -\rho\nabla\cdot\boldsymbol{u}, \quad p = f(\rho) \\ \dfrac{D\boldsymbol{u}}{Dt} = \dfrac{1}{\rho}\nabla p + \dfrac{1}{\rho}\nabla\cdot\mathbb{V} + \boldsymbol{g}\,, \end{cases} \tag{1}$$

where $\rho$ and $\boldsymbol{u}$ are respectively the density and velocity of the fluid, $\mathbb{V}$ is the viscous stress-tensor and $p$ and $\boldsymbol{g}$ represent the pressure and body forces respectively.

Based on the weakly-compressible assumption, pressure is determined as a function of density fluctuations through an Equation of State (EOS). In particular, in this work a simple linearised EOS is chosen, such that:

$$p = c_0^2\left(\rho - \rho_0\right)\,. \tag{2}$$

Viscous stress-tensor, for a Newtonian fluid, can be rewritten in the form:

$$\mathbb{V} = \lambda\, tr(\mathbb{D})\,\mathbb{I} + 2\mu\mathbb{D}\,, \tag{3}$$

where $\mathbb{D}$ is the strain rate tensor, $\mathbb{D} = (\nabla\boldsymbol{u} + \nabla\boldsymbol{u}^T)/2$, $\mathbb{I}$ the Identity tensor and $\lambda$ and $\mu$ the bulk and dynamic viscosity coefficients respectively.

In SPH, the $\delta$-SPH model proposed by [2], has been revisited in [11] from a LES-perspective. The $\delta$-LES-SPH model has been later extended in [14] and [15] and is the one used in this work. The set of Equations in (1) turn into:

$$\begin{aligned} &\frac{D\rho_i}{Dt} = -\rho_i\sum_j(\boldsymbol{u}_j - \boldsymbol{u}_i)\cdot\nabla W_{ij}V_j \\ &+hc_s\sum_j \delta_{ij}\mathcal{D}_{ij}\cdot\nabla W_{ij}V_j\,, \\ &\frac{D\boldsymbol{u}_i}{Dt} = \boldsymbol{g} - \frac{1}{\rho_i}\sum_j\left(p_i + p_j\right)\nabla W_{ij}V_j \\ &+hc_s\frac{\rho_0}{\rho_i}\sum_j\alpha_{ij}\Pi_{ij}\nabla W_{ij}V_j\,, \end{aligned} \tag{4}$$

where $\mathcal{D}_{ij}$ is the diffusive term added to the continuity equation in the standard $\delta$-SPH model [2] and $\Pi_{ij}$ the viscous part of the momentum equation, which are expressed as:

$$\begin{aligned} &\mathcal{D}_{ij} = 2\left[(\rho_j - \rho_i)\right. \\ &\left.-\frac{1}{2}\left(\langle\nabla\rho\rangle_j^L + \langle\nabla\rho\rangle_i^L\right)\cdot(\boldsymbol{r}_j - \boldsymbol{r}_i)\right]\frac{(\boldsymbol{r}_j - \boldsymbol{r}_i)}{\|\boldsymbol{r}_j - \boldsymbol{r}_i\|^2}, \\ &\Pi_{ij} = \frac{(\boldsymbol{u}_j - \boldsymbol{u}_i)\cdot(\boldsymbol{r}_j - \boldsymbol{r}_i)}{(\boldsymbol{r}_j - \boldsymbol{r}_i)^2}\,, \end{aligned} \tag{5}$$

where $\langle\nabla\rho\rangle_i^L$ represents the renormalized density gradient, as defined in [16].

Actually, the main difference of the $\delta$-LES-SPH model comes from the fact that diffusive coefficients $\delta$ and $\alpha$ acting in each equation are no longer considered as constants, but being computed on each particle and having physical meaning. The new $\delta_{ij}$ quantity is computed as:

$$\delta_{ij} = 2\,\frac{\delta_i\,\delta_j}{\delta_i + \delta_j}\,, \tag{6}$$

where,

$$\delta_i = \frac{\nu_i^\delta}{c_s h}\,, \tag{7}$$

and

$$\nu_i^\delta = (C_\delta L_{LES})^2\|\mathbb{D}\|_i\,, \tag{8}$$

in which $C_\delta$ is a constant equal to 1.5 and $L_{LES}$ is a reference length for the SPH filtering procedure, that is set equal to the SPH kernel radius, in our case $L_{LES} = 2h$. The quantity $\|\mathbb{D}\|_i$ is given by:

$$\|\mathbb{D}\|_i = \sqrt{2\mathbb{D}_i : \mathbb{D}_i}, \tag{9}$$

that is computed as:

$$\begin{aligned} \mathbb{D}_i = \frac{1}{2}\sum_j &\left[(u_j - u_i)\otimes(\mathbb{L}_i\cdot\nabla W_{ij})\right. \\ &\left.+(\mathbb{L}_i\cdot\nabla W_{ij})\otimes(u_j - u_i)\right]V_j, \end{aligned} \tag{10}$$

where $\mathbb{L}_i$ is the is the tensor for correcting the kernel gradient in order to recover the first-order completeness [16].

Analogously, the viscous coefficient $\alpha_{ij}$ becomes a function of the interacting particles. It can be expressed in the following form:

$$\alpha_{ij} = \alpha + 2\,\frac{\alpha_i \alpha_j}{\alpha_i + \alpha_j}\,, \tag{11}$$

where $\alpha$ is the contribution due to real viscosity, whilst $\alpha_i$ accounts for a turbulent viscosity contribution:

$$\alpha_i = \alpha + \frac{K\nu_i^{\alpha}}{c_s h \rho_0}\,, \tag{12}$$

where $K$ is a constant that is set to 8 or 10 depending on the simulation being 2-D or 3-D respectively, and,

$$\nu_i^{\alpha} = (C_{\alpha} L_{LES})^2 \|\mathbb{D}\|_i\,, \tag{13}$$

in which $C_{\alpha}$ is the Smagorinsky constant, which takes the value of $0.12$.

Regarding the boundary treatment, numerical boundary integrals [10] are used for the problems tested, implemented according to [7]. In the boundary integrals formulation, the differential operators from (1) are defined in the presence of a boundary as:

$$\langle \nabla f \rangle_i = \frac{1}{\gamma_i} \sum_j f_j \cdot \nabla W_{ij} V_j + \sum_j f_j \cdot \boldsymbol{n}_j W_{ij} s_j\,, \tag{14}$$

where $f_j$ is a generic field function, $\boldsymbol{n}_j$ the normal to the surface, pointing outwards, $s_j$ the area of the surface element and $\gamma_i$ the Shepard renormalization factor, that in this case is computed according to the procedure described in [7].

### *B. Beam model*

The equation for a beam is given by the Euler-Bernoulli beam theory as:

$$m(x)\frac{\partial^2 w(x,t)}{\partial t^2} + c\frac{\partial w(x,t)}{\partial t} + EI\frac{\partial^4 w(x,t)}{\partial x^4} = f(x,t)\,, \tag{15}$$

where $x$ is the spatial coordinate whilst $t$ the time. $m(x)$ is the distributed mass of the beam (in the future the mass will be assumed as a constant distribution $m(x) = m$), $w$ the vertical displacement, $c$ accounts for the internal damping of the beam, $EI$ is the structural rigidity and $f(x,t)$ a generalized force.

There are several possibilities to model such a problem. Although numerical solutions, such as finite-differences, finite-element or even SPH are a popular standard, as in this case we are not so much interested in computing accurately physical phenomena, such as stress or elongations within the beam, but to analyse the influence of the external loading on the beam movement, and how this modifies fluid behaviour inside the tank, a more simple solution is sought. Therefore, two possibilities have been chosen. The most simplest model consists on modelling the beam as a mass-spring-damper system. Therefore, equation (15) can be written as:

$$m\ddot{w} + c\dot{w} + Kw = f(t)\,, \tag{16}$$

where $m$ and $c$ have been already defined, and $K$ is the stiffness. This way, the solution now only depends on the temporal discretization. For a cantilever beam, the stiffness due to vertical motion takes the form $K = 3\,E\,I/L^3$. To obtain the damping, the system can be rearranged as:

$$\ddot{w} + 2\xi\omega\dot{w} + \omega^2 w = f(t)\,, \tag{17}$$

where $\omega$ is the natural frequency of the system $\omega = \sqrt{K/m}$ and $\xi$ is the damping coefficient. Identifying terms between Eqs. (16) and (17), the value of $c$ can be established.

This solution, although simple and robust, considers the beam as an only moving point, and therefore no local displacements are considered. This implies that rolling motion is not included in the model, which might be relevant for the sloshing flow in some conditions.

Another possibility for the solution to Equation (15) can be given according to the following expression:

$$w(x,t) = \sum_i^n \phi_i(x) q_i(t)\,, \tag{18}$$

which means that the problem can be split up into two different problems, one to solve the spatial discretization and another to solve the temporal evolution. Substituting Eq. (18) into Eq. (15), and considering the homogeneous solution, one gets:

$$m\,\phi(x)\ddot{q}(t) + c\,\phi(x)\dot{q}(t) + EI\,\phi^{IV}(x) q(t) = 0. \tag{19}$$

Equation (19) can be split into two different problems, given by:

$$\frac{EI}{m}\frac{\phi^{IV}(x)}{\phi(x)} = \frac{c}{m}\frac{\dot{q}(t)}{q(t)} + \frac{\ddot{q}(t)}{q(t)} = \lambda^2. \tag{20}$$

This implies that the two differential equations to be solved are:

$$\begin{aligned} &\phi^{IV}(x) - k_n^4 \phi(x) = 0 \\ &\ddot{q}(t) + \frac{c}{m}\dot{q}(t) + \lambda^2 q(t) = 0\,, \end{aligned} \tag{21}$$

where $k_n^4 = \frac{\lambda^2}{a^2}$ and $a^2 = \frac{EI}{m}$.

Regarding the spatial discretization from Eq. (21), we assume a solution of the form [13]:

$$\phi(x) = C_1 cosh(kx) + C_2 cos(kx) + C_3 sinh(kx) + C_4 sin(kx). \tag{22}$$

To solve this equation four boundary conditions are needed. For a cantilever beam (fixed end at $x = 0$ and free end at $x = L$), these take the following form:

$$\begin{aligned} &w(0,t) = X(0) = 0 \qquad \frac{\partial w(0,t)}{\partial x} = \frac{\partial X(0)}{\partial x} = 0 \\ &\frac{\partial^2 w(L,t)}{\partial x^2} = \frac{\partial^2 X(L)}{\partial x^2} = 0 \qquad \frac{\partial^3 w(L,t)}{\partial x^3} = \frac{\partial^3 X(L)}{\partial x^3} = 0\,. \end{aligned} \tag{23}$$

Applying Eq. (23) to the expression in Eq. (22), the general solution is:

$$\begin{aligned} &\phi_i(x) = cosh(k_i x) - cos(k_i x) \\ &-\beta_i \left(sinh(k_i x) - sin(k_i x)\right)\,, \end{aligned} \tag{24}$$

with

$$\beta_i = \frac{cosh(k_i L) - cos(k_i L)}{sinh(k_i L) - sin(k_i L)}. \tag{25}$$

As it has been mentioned, $k_i$ is a function of the natural frequency. For a cantilever beam, it can be known from the solutions of the following expression:

$$cos(k_n x)cosh(k_n x) = -1. \tag{26}$$

The solution for the first five modes for $k_i$ and $\alpha_i$ can be found in Table I.

TABLE I
SOLUTION FOR THE FIRST FIVE MODES OF $k_i$ AND $\alpha_i$

| **Mode** | 1 | 2 | 3 | 4 | 5 |
|---|---|---|---|---|---|
| $k_i$ | 1.875 | 4.694 | 7.854 | 10.995 | 14.137 |
| $\alpha_i$ | 0.734 | 1.018 | 0.999 | 1.000 | 0.999 |

Once the spatial solution has been found, and the eigenmodes and their corresponding natural frequencies are known, the time-dependant solution can be sought from the second Equation in (21).

The force term can be added at this point. The general force considered in this work is a set of concentrated forces acting at determined points along the beam.

$$\begin{aligned} f(x,t) = \sum_{k}^{m} F_k \delta(x - c_k)\delta(t - t_0) = \\ \sum_{k}^{m}\sum_{i}^{n} \phi_i(x) F_k \phi_i(c_k)(t - t_0). \end{aligned} \tag{27}$$

The complete system in (21) can now be solved and the total displacement at each time step computed. In this work, a 4th-order Runge-Kutta algorithm in time is used.

### C. Coupling

As it has been seen in previous sections, to obtain displacements, velocities and accelerations in the beam, an input force is needed. This force is actually the fluid force acting on the tank and being transmitted to the beam. The forces are obtained from the SPH solver according to $F_{body/fluid} = F^p_{body/fluid} + F^V_{body/fluid}$, where:

$$\begin{cases} F^p_{body/fluid} & := & \displaystyle\int_{\partial\Omega_B} \boldsymbol{dF}^p\,, & \vec{dF}^p := -p\,\boldsymbol{n}\,dS, \\ F^V_{body/fluid} & := & \displaystyle\int_{\partial\Omega_B} \boldsymbol{dF}^V\,, & \vec{dF}^V := 2\,\mu\,\mathbb{D}\cdot\boldsymbol{n}\,dS, \end{cases} \tag{28}$$

with $\boldsymbol{F}_{body/fluid}$ being the total force applied by the body on the fluid and $\boldsymbol{F}^p_{body/fluid}$, $\boldsymbol{F}^V_{body/fluid}$ the corresponding pressure and viscous components.

According to the boundary integrals formulation, these forces can be expressed in the SPH model as:

$$\begin{aligned} F^p_{body/fluid} &= -\sum_i \sum_j V_i\, S_j\ (p_j + p_i)\,\boldsymbol{n}_j W_{ij}, \\ F^V_{body/fluid} &= \sum_i \sum_j V_i\, S_j \mu\, \pi_{ij}\cdot \boldsymbol{n}_j W_{ij}. \end{aligned} \tag{29}$$

In order to simplify the process, the tank is assumed to be perfectly attached to the beam, and therefore forces can only be transmitted through two supports located at the bottom ends of the tank, as it is depicted in Figure 2.

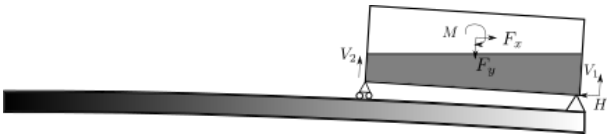


Fig. 2. Forces equilibrium diagram. $F_x$, $F_y$ and $M$ are the forces and moment coming out from the fluid, and $H$, $V_1$ and $V_2$ the reactions.

Forces and reactions are set according to:

$$\begin{aligned} \sum \boldsymbol{F} &= m_t \ddot{w}\,, \\ \sum \boldsymbol{M} &= I_t \alpha\,, \end{aligned} \tag{30}$$

where $m_t$ is the mass of the tank, $\ddot{w}$ the acceleration of the system, $I_t$ the inertia of the tank and $\alpha$ its angular acceleration.

### D. Energy Analysis

In this section, an analysis of the sources of energy dissipation of the numerical fluid system is discussed. The First Law of Thermodynamics, i.e. the conservation of energy, can be stated as follows [8]:

$$\frac{\mathrm{d}\varepsilon_I}{\mathrm{d}t} + \frac{\mathrm{d}\varepsilon_M}{\mathrm{d}t} = \mathcal{P}_{body/fluid}\,, \tag{31}$$

where $\varepsilon_I$ and $\varepsilon_M$ are respectively the internal and mechanical energies of the fluid, while $\mathcal{P}_{body/fluid}$ is the power delivered by the solid boundary $\partial\Omega_B$ to the fluid. The power $\mathcal{P}_{body/fluid}$ can be obtained by integrating the elementary power acting on each surface element of $\partial\Omega_B$:

$$\mathcal{P}_{body/fluid} = \int_{\partial\Omega_B} (\mathbb{T}\cdot\boldsymbol{n})\cdot\boldsymbol{u}_B\,dS, \tag{32}$$

where $\mathbb{T}$ is the stress tensor and $\boldsymbol{u}_B$ is the velocity of the body.

For a Newtonian fluid, the stress tensor reads:

$$\mathbb{T} = (-p\ +\ \lambda\, tr\ (\mathbb{D}))\ \mathbb{I} + 2\,\mu\,\mathbb{D}\,. \tag{33}$$

Using equation (33), we can split $P_{body/fluid}$ in two components, one associated to the pressure field and the other to the viscous forces, as it has already been done, where:

$$\begin{cases} \mathcal{P}^p_{body/fluid} & := & \displaystyle\int_{\partial\Omega_B} \boldsymbol{u_B}\cdot\boldsymbol{dF}^p\,, \\ \mathcal{P}^V_{body/fluid} & := & \displaystyle\int_{\partial\Omega_B} \boldsymbol{u_B}\cdot\boldsymbol{dF}^V\,, \end{cases} \tag{34}$$

with $\boldsymbol{dF}^p$ and $\boldsymbol{dF}^V$ being the elementary pressure and viscous forces of the body surfaces acting on the fluid, which have already been defined in previous section.

On the left hand side of Equation (31), there is the mechanical energy $\epsilon_M$, which can be split as the sum of kinetic and potential energies. Each of these can be expressed in the SPH framework for the particle system as:

$$\epsilon_k = \frac{1}{2}\sum_i m_i \|u_i\|^2 \qquad \epsilon_p = -\sum_i m_i \boldsymbol{g}\cdot\boldsymbol{r}_i\,. \tag{35}$$

Under the assumption of weakly-compressibility, the constitutive equation for the internal energy $\varepsilon_I$ is:

$$\frac{\mathrm{d}\varepsilon_I}{\mathrm{d}t} = \frac{\mathrm{d}\varepsilon_C}{\mathrm{d}t} - \mathcal{P}^V \,, \tag{36}$$

where $P^V$ is the viscous dissipation rate of the fluid (which is always negative in the theoretical model, consistently with the Second Law of Thermodynamics), and where $\varepsilon_C$ is the elastic energy of the fluid due to the compressibility, i.e.:

$$\frac{\mathrm{d}\varepsilon_C}{\mathrm{d}t} = \sum_i V_i \frac{p_i}{\rho_i} \frac{\mathrm{d}\rho_i}{\mathrm{d}t}, \tag{37}$$

On the other hand, the viscous dissipation rate of the fluid $P^V$ can be split as the sum of the different sources of dissipation in the model, this is, dissipation due to $\delta$ term, dissipation due to $\alpha$ term, and the dissipation due to the boundaries. Both $\delta$ and $\alpha$ dissipation terms can be expressed as:

$$\begin{aligned} \mathcal{P}_\delta &= -hc \sum_i \frac{p_i}{\rho_i} \sum_j \mathcal{D}_{ij} V_j V_i \\ \mathcal{P}_\alpha &= hc\rho_0 \sum_i \sum_j \Pi_{ij} (\boldsymbol{u}_j - \boldsymbol{u}_i) \nabla W_{ij} V_i V_j . \end{aligned} \tag{38}$$

Finally, the dissipation term due to the boundaries $\mathcal{P}_s$, as discussed in [1], depends on the technique used at the boundaries. In [9] the different solutions are drafted. For the boundary integrals technique proposed here, this term becomes:

$$\begin{aligned} \mathcal{P}_s = \frac{1}{\gamma_i} \sum_i \sum_j V_i \left[ \mu \Pi_{ij} \boldsymbol{u}_i + (p_i + p_j) \boldsymbol{u}_i \right. \\ \left. + p_i (\boldsymbol{u}_j - \boldsymbol{u}_i) \right] \cdot \boldsymbol{n}_j W_{ij} s_j . \end{aligned} \tag{39}$$

Rearranging the terms derived in the two previous subsections, the rate of variation of the total internal energy of the fluid can be written as follows:

$$\frac{\mathrm{d}\varepsilon_M}{\mathrm{d}t} + \frac{\mathrm{d}\varepsilon_C}{\mathrm{d}t} - (\mathcal{P}_\delta + \mathcal{P}_\alpha + \mathcal{P}_s) = \mathcal{P}^V_{body/fluid} + \mathcal{P}^p_{body/fluid}. \tag{40}$$

## III. Preliminary Results

### A. Static test

In order to test the two beam models presented above and to set the different constants to model appropriately the beam, a static test is performed at first. For this test the beam is set at rest and is loaded with different masses until a steady value of deflection is reached. Figure 3 presents results of both models presented in previous Section versus the experimental values. Values for the models are chosen to set the same rigidity found out in experiments, meaning $E = 210\,GPa$, $I = 5.57e^{-7}\,m^4$ and an effective length $L_b = 2.48\,m$. From measurements, it is found that the linear mass of the beam is $\rho_b = 13.04\,kg/m$, and therefore the total mass is $32.34\,kg$. As it can be appreciated, both models reproduce accurately the results from the experiment for the static test.

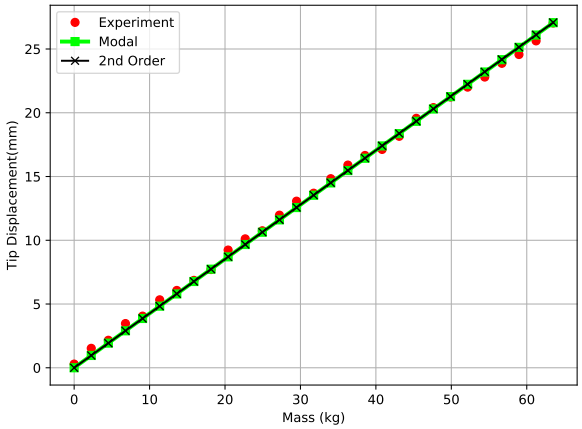


Fig. 3. Displacement at the tip for the static test.

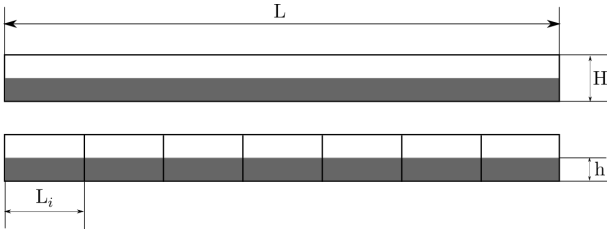


Fig. 4. Geometry of the two configurations tested: rectangular tank (top) and baffled tank (bottom).

### B. Dynamic Tests

Once the beam parameters are known, a set of dynamic tests is performed.

For the dynamic tests, the tank is attached to the beam, therefore modifying the properties of the system. Two configurations for the tank are tested: a rectangular tank and a baffled tank. Geometries for both configurations can be seen in Figure 4. The total length of the tank is $L = 0.7\,m$ and height $H = 0.06\,m$. Baffled tank is composed by 7 compartments with length $L_i = 0.1\,m$. The total length of the tank in this case is extended to $L = 0.73\,m$, so both configuration have the same amount of fluid for a determined filling level. Filling level $h$ can be varied, although in this work only results for filling level $h = 50\%\,H$ will be presented.

The beam is pre-loaded and let oscillate freely, and motion, velocity and acceleration is measured. In this set of cases, the initial displacement at the tip is always the same, corresponding to $w_{tip} = 0.04\,m$ In order to establish a comparison reference, first a preliminary test without liquid is carried out. Instead of liquid, a solid mass with a weight corresponding to a 80% filling condition (the maximum tested) is attached inside the tank. All tests carried out in this work have the same total nominal mass, which is the corresponding to the sum of the different systems. Therefore, a ballast mass is added for the $50\%$ filling level, corresponding to the remaining mass.

Figure 5 shows raw acceleration data obtained from the

experiments, and those calculated with the model. Damping coefficient in the model has been set to 1.5%, which is a standard value found out in the computation of structural models, such as bridges. From this Figure it can be observed that although the model response decays homogeneously, contrary to the experiment register where a more chaotic signal is obtained, both results show that accelerations lie in the same order of magnitude, and that their behaviour is similar.

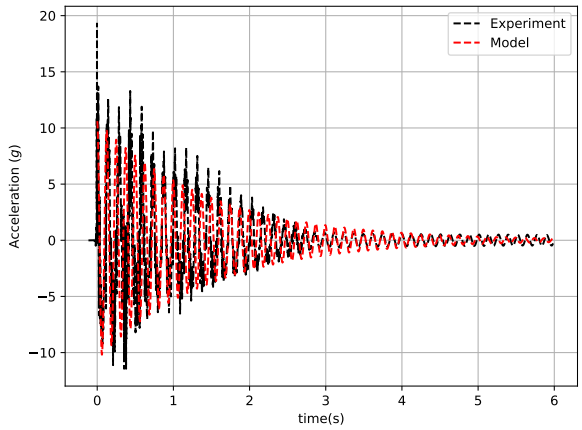


Fig. 5. Acceleration registered for the modelled beam and the experimental beam for the solid mass test case without liquid.

Once the model with a solid mass is tested, some tests to compare the behaviour of sloshing fluid for the two inner configurations are shown. In these cases presented, tank motion is purely vertical, and no angle is induced on the tank, but the effect of fluid force on the response can be drafted. Results for the sloshing fluid are shown in Figures 6 and 7. In these Figures, the evolution of the turbulent kinetic energy in log scale at five different relevant moments of the simulation is shown. Resolution in Figure 6 is set as $L/dr = 2000$ and in Figure 7 as $L_i/dr = 360$. Compact support and speed of sound are chosen the same for both tests, such that $h/dr = 2$ and $c_s = 20\,m/s$. As the tank motion is purely vertical, fluid behaviour is pretty similar at the first stages of the simulation for both tests. However, as the motion dampens, a wave is generated in the horizontal direction, and the vertical baffles play a role as they do not allow the wave to propagate. Nonetheless, there is not a noticeable influence on the turbulent kinetic energy field values.

Similarly to Figure 5, in Figure 8, accelerations registered in the experiments are compared to the numerical results obtained from the 50% filling level case for the baffled configuration. At first stages experimental data values do not match very well with numerical obtained solution, reaching values over $11\,g$, the maximum theoretically predicted. However, then the signals tend to similar accelerations when the motion starts to dampen.

Motion damping due to fluid force is one of the key aspects to analyse in this work. In order to find a clearer comparison

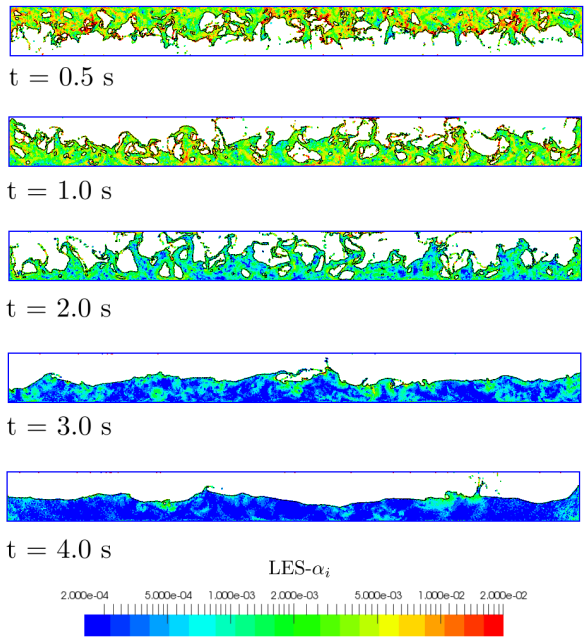


Fig. 6. Evolution of the turbulent intensity in the fluid at five different moments of the simulation with the $\delta$-LES-SPH model. Rectangular tank with 50% filling level.

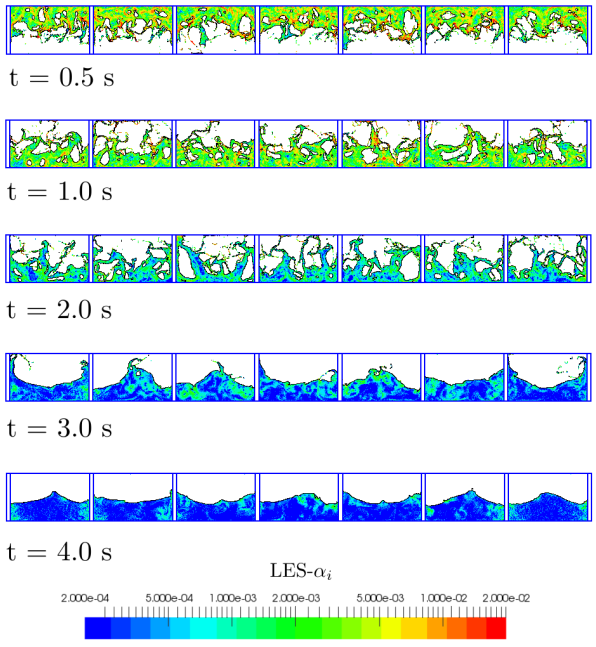


Fig. 7. Evolution of the turbulent intensity in the fluid at five different moments of the simulation with the $\delta$-LES-SPH model. Baffled tank with 50% filling level.

between the solid mass and the fluid sloshing tests regarding damping, in Figure 9 the non-dimensional motion time history

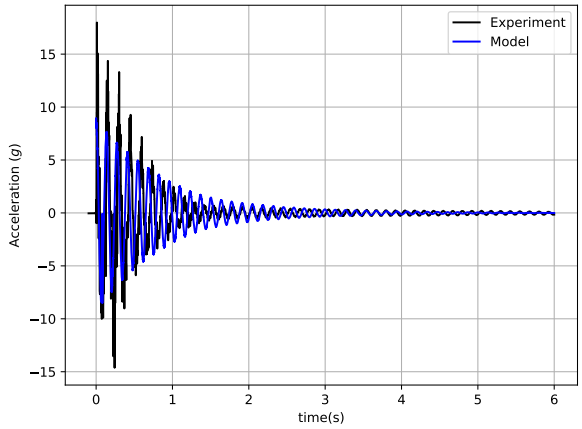


Fig. 8. Acceleration registered for the modelled beam and the experimental beam for the 50% filling level baffled case.

for both the solid mass case and the fluid case obtained from the simulations is shown. As it can be seen, damping is stronger when the fluid sloshes, reaching first a stationary motion.

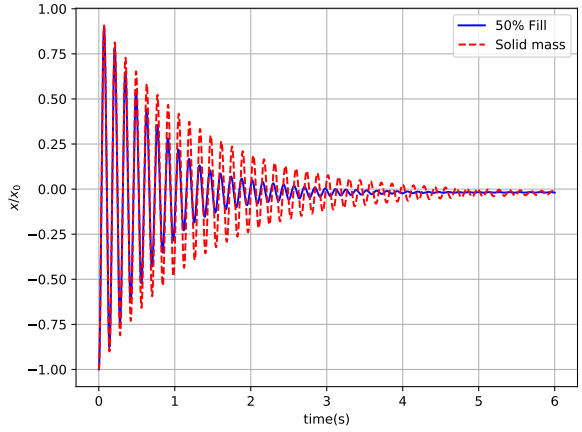


Fig. 9. Non-dimensional motion for the beam: red dashed line represents the solid mass motion, blue solid line represents the 50% fill fluid motion. $x_0 = x(t = 0)$.

In Figure 10 this effect is emphasized. It shows the envelope of the acceleration register amplitude for the two cases presented in Figure 9. Damping can be obtained from the slope of the curves. At first stages, this damping is bigger for the fluid sloshing case, and then, once the motion is sufficiently damped, both curves follow approximately the same trend, showing that fluid sloshing role loses importance and is the damping of the beam that mainly contributes to the decay in motion. This is in accordance with the fluid evolution observed in Figures 6 and 7.

Another important analysis is how the energy in the fluid evolves during the simulation. In Figure 11 the different energy components at the tank for the simulation with 50% filling

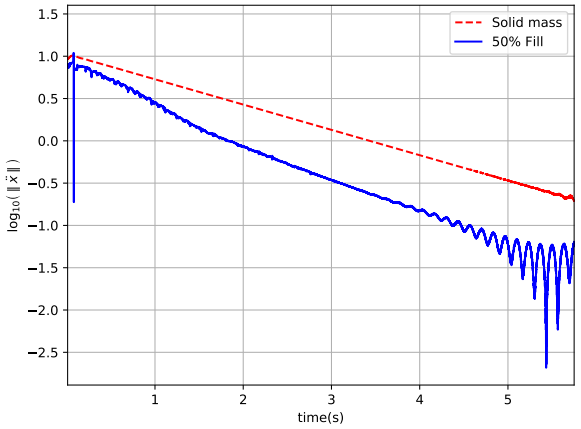


Fig. 10. Envelope of the acceleration register for the solid mass motion test (red dashed line) and the 50% filling fluid test (blue solid line).

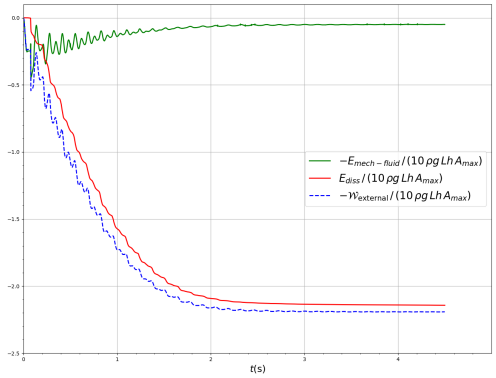


Fig. 11. Energy analysis: green line represents the evolution of mechanical energy, red line corresponds to the evolution of dissipation terms, whilst blue line is the external work contribution.

level is shown. As it can be appreciated, in the same fashion as what is observed from previous results, there exist sharp increases in the forces and dissipation terms every time the fluid hits a wall. This can be also appreciated in variations of mechanical energy. Once motion is dampened, contributions remain stable, keeping the energy terms constant. Energy is therefore conserved.

## IV. Conclusions

In this work, a numerical model of a fully coupled fluid-structure interaction problem is developed. The aim is to analyze damping effects due to liquid sloshing inside fuel tank of aircraft wings. In order to reproduce experimental results, fluid is simulated through the $\delta$-LES-SPH model, implemented in the boundary integrals methodology framework. The structure is modelled through beam theory. Two different models based on this theory have been presented From the results presented, the main conclusions from this work are: first, that

SPH as numerical tool is able to confirm that the presence of liquid in the tanks attached to flexible structures introduces a damping effect that can be numerically measured in terms of motion and compared to the experiments. Second, that SPH is able to model complex baffled geometries involving several phenomena at the same time through the boundary integrals approach, and finally, that the coupled system is able to capture the energy mechanisms and transfers involved in the phenomenon.

Despite the promising results, there are still efforts to be made in several directions. Models are limited to 1-D, for the case of the mass-spring-damper system, and 2-D for the modal solution. More degrees of freedom can be added in order to set accurately the motions in complex situations. Although a considerable resolution has been used, there is still a need for further refinement in order to capture as much turbulent phenomena as possible. The current work relies mainly on 2-D simulations. However, it has been previously assessed that 3-D effects may play a role in the damping mechanisms, especially when inner baffled configurations are introduced.

## ACKNOWLEDGMENTS

This research is receiving funding from European Union (EU) under H2020 grant 815044 "*Sloshing Wing Dynamics (SLOWD)*" .

The authors also acknowledge the financial support from the Spanish Ministry for Science, Innovation and Universities (MCIU) under grant RTI2018-096791-B-C21 "*Hidrodinámica de elementos de amortiguamiento del movimiento de aerogeneradores flotantes*".

This research has also received funding from Universidad Politécnica de Madrid under a pre-doctoral scholarship.

## REFERENCES

[1] M. Antuono, S. Marrone, A. Colagrossi, and B. Bouscasse, "Energy balance in the $\delta$-SPH scheme," *Computer methods in Applied Mechanics and Engineering*, 2015.

[2] M. Antuono, A. Colagrossi, and S. Marrone, "Numerical diffusive terms in weakly-compressible SPH schemes," *Computer Physics Communications*, vol. 183, no. 12, pp. 2570–2580, 2012.

[3] T. O. Arndt and M. E. Dreyer, "Damping behavior of sloshing liquid in laterally excited cylindrical propellant vessels," *Journal of Spacecraft and rockets*, vol. 45, no. 5, pp. 1085–1088, 2008.

[4] B. Bouscasse, A. Colagrossi, A. Souto-Iglesias, and J. Cercos-Pita, "Mechanical energy dissipation induced by sloshing and wave breaking in a fully coupled angular motion system. I. theoretical formulation and numerical investigation," *Physics of Fluids*, vol. 26, no. 3, p. 033103, 2014.

[5] ——, "Mechanical energy dissipation induced by sloshing and wave breaking in a fully coupled angular motion system. II. experimental investigation," *Physics of Fluids*, vol. 26, no. 3, p. 033104, 2014.

[6] G. Bulian, A. Souto-Iglesias, L. Delorme, and E. Botia-Vera, "Smoothed particle hydrodynamics (SPH) simulation of a tuned liquid damper (TLD) with angular motion," *Journal of Hydraulic Research*, vol. 47, no. extra issue, pp. 28–39, 2009.

[7] J. Calderon-Sanchez, J. Cercos-Pita, and D. Duque, "A geometric formulation of the shepard renormalization factor," *Computers & Fluids*, vol. 183, pp. 16 – 27, 2019.

[8] J. Cercos-Pita, M. Antuono, A. Colagrossi, and A. Souto-Iglesias, "SPH energy conservation for fluid–solid interactions," *Computer Methods in Applied Mechanics and Engineering*, 2017.

[9] J. L. Cercos-Pita, "A novel generalized diffusive SPH model: Theoretical analysis and 3D HPC implementation," Ph.D. dissertation, 2016.

[10] ——, "Aquagpusph, a new free 3D SPH solver accelerated with OpenCL," *Computer Physics Communications*, vol. 192, pp. 295–312, 2015.

[11] A. Di Mascio, M. Antuono, A. Colagrossi, and S. Marrone, "Smoothed particle hydrodynamics method from a large eddy simulation perspective," *Physics of Fluids*, vol. 29, no. 3, p. 035102, 2017.

[12] F. Gambioli, "Fuels loads in large civil airplanes," in *4th ERCOFTAC SPHERIC workshop on SPH applications*, 2009.

[13] M. L. James, G. M. Smith, J. Wolford, and P. Whaley, *Vibration of mechanical and structural systems: with microcomputer applications*. Harper Collins, 1994.

[14] D. D. Meringolo, Y. Liu, X.-Y. Wang, and A. Colagrossi, "Energy balance during generation, propagation and absorption of gravity waves through the $\delta$-les-sph model," *Coastal Engineering*, vol. 140, pp. 355–370, 2018.

[15] D. D. Meringolo, S. Marrone, A. Colagrossi, and Y. Liu, "A dynamic $\delta$-sph model: How to get rid of diffusive parameter tuning," *Computers & Fluids*, vol. 179, pp. 334–355, 2019.

[16] P. Randles and L. Libersky, "Smoothed Particle Hydrodynamics: some recent improvements and applications," *Computer methods in applied mechanics and engineering*, vol. 39, pp. 375–408, 1996.

[17] A. Souto-Iglesias, L. P. Rojas, and R. Z. Rodríguez, "Simulation of anti-roll tanks and sloshing type problems with smoothed particle hydrodynamics," *Ocean Engineering*, vol. 31, pp. 1169–1192, 2004.

[18] A. Souto-Iglesias, L. Delorme, L. Pérez-Rojas, and S. Abril-Pérez, "Liquid moment amplitude assessment in sloshing type problems with smooth particle hydrodynamics," *Ocean Engineering*, vol. 33, pp. 1462–1484, 2006.

[19] M. Tait, "Modelling and preliminary design of a structure-tld system," *Engineering Structures*, vol. 30, no. 10, pp. 2644–2655, 2008.